Hydrodynamic Surface Interactions Enable *Escherichia Coli* to Seek Efficient Routes to Swim Upstream

Jane Hill,[1] Ozge Kalkanci,[2] Jonathan L. McMurry,[3] and Hur Koser[4]

[1]*Yale University, Department of Chemical Engineering, Environmental Engineering Program, Mason Laboratory, Room 318, New Haven, Connecticut 06520-8286, USA*

[2]*Bogazici University, Department of Biomedical Engineering, Bebek, Istanbul, Turkey*

[3]*Yale University, Molecular Biophysics & Biochemistry Department, 266 Whitney Avenue, New Haven, Connecticut 06520-8114, USA*

[4]*Yale University, Department of Electrical Engineering, 15 Prospect Street, Becton 507, New Haven, Connecticut 06520-8284, USA*

(Received 28 April 2006; published 6 February 2007)

Escherichia coli in shear flow near a surface are shown to exhibit a steady propensity to swim towards the left (within the relative coordinate system) of that surface. This phenomenon depends solely on the local shear rate on the surface, and leads to cells eventually aligning and swimming upstream preferentially along a left sidewall or crevice in a wide range of flow conditions. The results indicate that flow-assisted translation and upstream swimming along surfaces might be relevant in various models of bacterial transport, such as in pyelonephritis and bacterial migration in wet soil and aquatic environments in general.

DOI: 10.1103/PhysRevLett.98.068101 PACS numbers: 87.17.Jj, 87.16.Qp, 87.18.Ed

An *E. coli* bacterium has two to six flagella, which, when rotating counterclockwise, form a bundle that propels the cell forward (a ''run''). During a run, the flagellar bundle rotation is counterbalanced by cell body rotation in the opposite direction [1]. The propulsive force of the flagellar bundle is balanced by viscous fluid drag forces, and the bacterium swims at a steady speed until it tumbles [2]. Near a flat surface in a quiescent environment, conditions of force-free and torque-free swimming result in hydrodynamic trapping of motile *E. coli* [3,4]. The bacteria then exhibit extended run times [5,6], clockwise circular trajectories [3–7], and right-hand-side migration [8] along channel edges.

In experiments within macroscale flow-cell geometries [5,9,10], motile bacteria have been shown to exhibit random diffusive migration patterns [10], or to perform circular loops in the quiescent boundary layer of flow cells at high bulk flow rates [11]. Despite such preliminary studies, bacteria behavior under flow conditions near surfaces has not been fully characterized.

To investigate the hydrodynamics of flagellated bacteria in a flow environment, we constructed microfluidic devices via soft lithography [12] and subjected *E. coli* K12 cells to various flow regimes in a laminar flow channel that is 150 or 300 μm wide and between 50 and 450 μm deep. The main channel is preceded by three inlets, each connected via Teflon tubing to a syringe pump that varies input flow rates between 0.05 and 20 μL/min [see Figs. 1(a) and 1(b)].

Bacteria were introduced through the center inlet, suspended in solutions of either phosphate-buffered saline (PBS; *p*H 7) or Luria-Bertani (LB) broth. Either PBS or LB broth was injected into the side inlets. We observed that PBS resulted in substantial bacterial surface adhesion, whereas LB broth virtually eliminated cell attachment to the surface. When identical PBS solutions were pumped at equal flow rates from each inlet, the cells entering the main laminar flow channel through the center stream consistently showed a preference for adhesion towards the $-x$ direction (or ''left'') in the relative coordinate system of

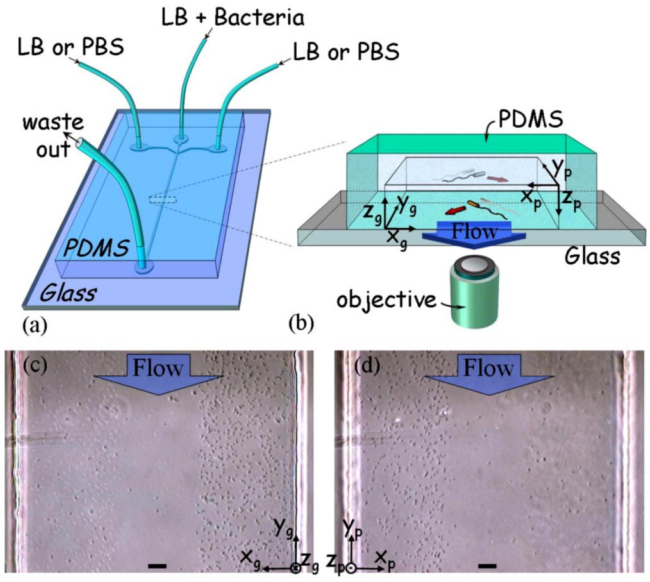

FIG. 1 (color online). *E. coli* cells in a laminar flow channel with three balanced inlets (a). Bacterial suspension is injected into the center inlet. (b) The central channel (width 150 or 300 μm, height 50–450 μm) receives the flows and is imaged from below. The bacteria attach with a $-x$ direction (or ''leftward'') bias on glass (c) and PDMS (d) surfaces when buffer (PBS) is injected into the side streams. Images are the average of 100 individual snapshots, resulting in the clear depiction of attached bacteria within the field of view. The scale bars represent 20 μm.

either the glass or polydimethylsiloxane (PDMS) surface [13]. The adhesion bias increased downstream. Introducing the bacteria with LB broth through the center stream significantly reduced bacterial attachment in the middle third of the channel near the inlets and clearly illustrated the directional bias in attachment [Figs. 1(c) and 1(d)]. Control experiments with fluorescein dye and microspheres confirmed balanced laminar flow streams in the main channel; experiments with unflagellated (YK4116) and paralyzed flagella (YK4183) *E. coli* K12 derivatives demonstrated that the attachment bias was only observed with the motile strain. Finally, introducing LB broth through all three inlets minimized attachment within the device (to a few adherents within the field of view over five hours), and we observed that most cells indeed swam consistently towards the negative x direction on either surface. LB broth was used exclusively in subsequent experiments in order to minimize surface-bacteria interactions and to study the swimming bias as a function of hydrodynamic factors alone.

We evaluated the response of motile *E. coli* K12 to changes in total volumetric flow rate in the main channel of the device between 0.15 and 60 μL/min over 20 s observation periods. With the bacterial body angle measured with respect to the x axis of either surface in Fig. 1, motile bacteria at each surface exhibited one dominant average angle [Figs. 2(a) and 2(b)], while the nonmotile YK4116 and YK4183 strains did not. The spread of the histograms in Figs. 2(a) and 2(b) is likely due to a combination of Brownian motion, bacterial "wobble" in the flagella bundle [1,2], variations in local hydrodynamic conditions across the channel width, and the effects of different bacteria lengths, as explained below.

Subdivision of each viewable surface into five equal sections illustrates the systematic effect of lateral position along the x axis on bacterial body angle [Fig. 2(c)]. Bacteria in the central section of either the top (PDMS) or the bottom (glass) surface were more perpendicular to the flow than those closer to the sidewalls. At the flow rate used in this example, variation in body angle across the channel width could be up to 17°. The angle distribution behavior in each section was essentially the same on either surface, with differences in angle data from each surface ultimately attributed to the asymmetry of the cross-section of deep channels [see Fig. 3(b)], as discussed later. Bacterial body angle was also a function of cell body aspect ratio [Fig. 2(d)]. Longer bacteria exhibited smaller angles when compared to shorter bacteria under the same

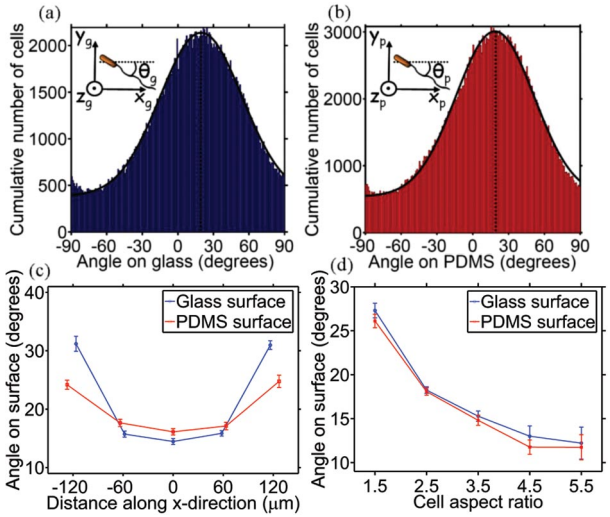

FIG. 2 (color). *E. coli* body angles at either surface of a 300 μm wide channel for a total flow rate of 9 μL/min. Average body angle is extracted via a Gaussian fit to the cumulative frequency histogram for *E. coli* cell bodies suspended in LB broth and imaged at the glass (a) and PDMS (b) surfaces. Bacterial body angle is measured in the x-y plane of the given surface. Here, the dominant body angle is 19.5° on glass and 18.5° on PDMS. (c) Average body angle within five equal-width sections across the surface width. The center point on either plot corresponds to the average angle in the middle strip of the respective surface; the PDMS surface is wider than glass for the channel cross-section in this example [see Fig. 3(b)]. (d) Average body angle as a function of cell aspect ratio. Error bars represent the 95% confidence interval in each peak position.

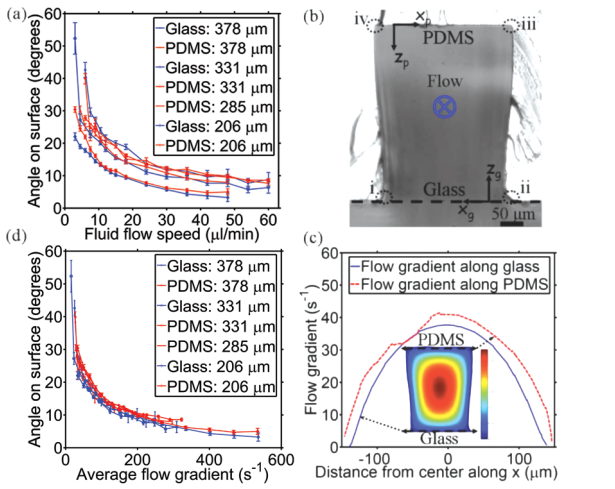

FIG. 3 (color). Shear rate along the z direction on the surface determines the body angle. (a) Average bacterial body angle in central channel strip near PDMS and glass surfaces as a function of flow rate for a 300 μm wide channel of variable depth (206–378 μm); deeper channels yield higher curves. (b) Cross section of device 7 mm from where the inlets meet to form the main channel, depicted here as an example. (c) Velocity field computed by COMSOL Multiphysics from different channel cross sections (shown here for the cross section in (b) for a flow rate of 9 μL/min) yields the shear rate in the z direction along each surface. Shear rate in the x-y plane over glass or PDMS is negligible compared to that along the z direction of either surface. (d) Average bacterial body angle as a function of average velocity gradient across that strip for several geometries. The angles for PDMS surface are virtually coincident with those for glass.

flow conditions (up to 14° under the flow rate used in Fig. 2).

Bacterial body angles were measured at the top and bottom surfaces of the channel along the central strip (to reduce spatial variation) for various flow rates in several channel geometries [Fig. 3(a)]. We observed that, for a given volumetric flow rate, bacteria were more perpendicular to flow as the channel narrowed. To understand why, cross sections of the PDMS stamps derived from the original template molds were imaged at each observation location [Fig. 3(b)], and a velocity field corresponding to each geometry and flow rate used in our experiments was computed via a 3D Navier-Stokes solver in COMSOL Multiphysics [Fig. 3(c)]. Reevaluation of body angles in the central strip using the average velocity gradient perpendicular to each surface (inside that strip) demonstrated coincident angles [Fig. 3(d)]. Average body angles at the glass surface are virtually the same as those at the PDMS surface, indicating that a given shear flow over a surface dictates the resultant angle. Other factors, such as specific device geometry (i.e., width and depth) and the roughness differences between the two surfaces, were not found to have a discernible systematic effect.

In the absence of flow, a motile bacterium near a surface exhibits a circular clockwise run trajectory, with its "nose," i.e., the end opposite the flagellar bundle, pointing slightly towards the surface plane [3,4,8] [Fig. 4(a)]. Under laminar flow and no-slip boundary conditions at the surface, steady-state bacterial body angles result from a balance of forces and torques, which are dominated by bacterial propulsion and fluid shear. Based on our observations, we propose that bacterial propulsion dominates over "slow" shear flow (up to about 10 s^{-1}), and the bacterium nose still dips towards the surface in this regime [Fig. 4(b)]. The increased drag around the nose then provides a pivot point around which the shear flow tends to orient the rest of the cell body to face upstream, much like a weather vane orienting in the wind. At two distinct angles [Figs. 4(b) (i) and (ii)], the clockwise torque (in the $-z$ direction) on the cell due to its swimming may be balanced by a hydrodynamic torque (which is counterclockwise at these angles). These angles are easily distinguishable in observations through periodic changes in the drift velocity of the cell as it gets dragged with the flow and translates to the right (i.e., $+x$ direction; see supplementary movies [14]). When fluid shear dominates, however, we propose that it is the downstream side of the cell body that dips slightly towards the surface at any bacterial angle in the x-y plane [15]. Torques along the z axis on the cell body due to shear flow and flagellar rotation balance in two similar angles, with either the nose or the flagella facing downstream [Fig. 4(c)]. However, we have observed that the dominant orientation is with the nose into the flow [Fig. 4(c) (i)], which results in translation to the left (i.e., $-x$ direction). We suggest that this angle prevails because, for the case depicted in Fig. 4(c) (ii), torque along the x axis resulting from the shear flow combines with the x-directed torque created by swimming, eventually flipping the cell. Net body movement is aided by the decrease in shear contribution as the bacterium approaches the sidewall [Fig. 3(c)]. There, *E. coli* migrating with the major angle [Fig. 4(c) (i)] translate upstream.

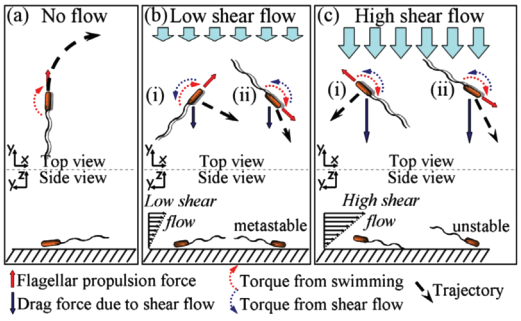

FIG. 4 (color). Some of the relevant hydrodynamic forces and torques acting on a motile bacterium near a surface and one possible mechanism that we propose to explain our observations. For clarity, axial torques on the cell body and the flagellar bundle, as well as viscous reaction forces and torques, are not shown. (a) In the absence of flow, the propulsive force of the flagella causes the nose of the cell to dip slightly, and the bacterium swims in a circular, clockwise trajectory at the surface [3,4]. (b) We propose that at low shear rates (~ 10 s^{-1} or less), flagellar propulsion still dominates and causes the nose to dip. The resulting hydrodynamic torque on the cell body along the z axis counterbalances the clockwise torque due to swimming at two distinct angles, (i) and (ii) (see text). (c) Shear flow rates above ~ 10 s^{-1} dominate over bacterial propulsion and the downstream end of the bacterium dips towards the surface. In this regime, bacteria drifting leftward and downstream at a stable angle (i) vastly outnumber others.

Nuances in channel geometry matter when bacteria under "high" shear flow over a surface reach a left sidewall. If the transition at the edge is relatively smooth (and the angle between surfaces is not acute—e.g., edges (iii) and (iv) in Fig. 3(b)], the bacteria will continue their leftward motion on the new surface. Indeed, in experiments with dilute bacteria solutions in shallow (50–100 μm deep) channels without trenches, we could manually track a given bacterium through the entire flow channel (over 4 cm), and we observed that the cells executed a left-handed helical motion around the inner periphery of the channel as they drifted downstream. This trajectory enables *E. coli* to "locate" flow regimes more favorable to upstream swimming within the device [typically in acute angle trenches where neighboring surfaces meet; Fig. 3(b) (i),(ii)]. Bacteria entering these crevices swim upstream in single file (Fig. 5). In experiments, we observed that *E. coli* tended to swim upstream mostly along the left edge of the glass surface [edge (ii) of Fig. 3(b)]. This preference may be because swimming upstream in the left trench is hydrodynamically stable; a bacterium tending to move out away

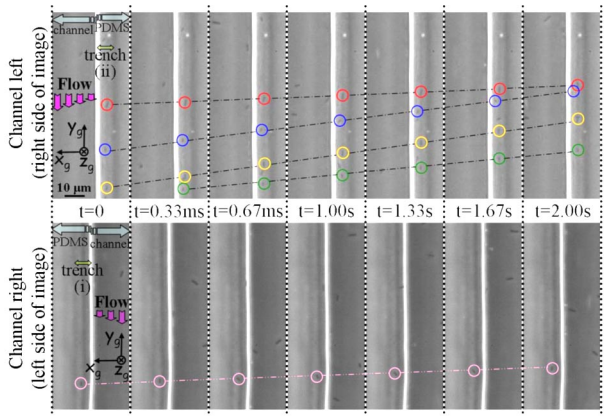

FIG. 5 (color online). Bacteria imaged within the narrow trenches [such as (i) and (ii) depicted in Fig. 3(b)] between the glass surface and the PDMS side walls of a microfluidic channel that is 150 μm wide and 93 μm deep. At most flow rates, the vast majority of cells within either trench swim upstream. Cells show a specific preference for the trench under the left sidewall along the glass surface [i.e., trench (ii) in Fig. 3(b); top row of images]. The sequential images depicted here correspond to a 2 s interval for a total flow rate of 3 μl/ min. The images show cells swimming upstream at different speeds.

from the sidewall will feel increased shear forces that quickly cause it to swim left, returning it to the trench.

The hydrodynamic surface interactions of motile *E. coli* depend mainly on the local shear flow rate—as such, we propose that the phenomenon described here will be observable in any flow channel of arbitrary cross section where surface-bacterial interactions do not interfere substantially with the hydrodynamic effects. Such hydrodynamic interactions will enable *E. coli* and other peritrichously flagellated bacteria (e.g., *Salmonella spp.*) to seek efficient routes to swim upstream in a wide range of flow conditions. Multiple morphologies and variable propulsion speeds within a given cell population may point to their having an evolutionary advantage (e.g., increase in pathogenicity) in the presence of a wide range of flow regimes. Flow-assisted translation in micro- and macroscale models of bacterial transport should be considered, even where bulk flow Reynolds numbers are larger than unity, since flow right at the surface may be laminar enough to accommodate this phenomenon. In particular, upstream swimming of bacteria might be relevant to the transport of *E. coli* in the upper urinary tract (leading to pyelonephritis) [16], infection in catheterized patients [17,18], the incidence of microbial contamination at protected wellheads [19,20], and biofilm formation [21,22] in flow channels. In addition, the ability to sort flagellated cells based on their size, shape, and swim speed in simple flow chambers could have numerous biomedical applications.

[1] H. C. Berg, Phys. Today **53**, No. 1, 24 (2000).
[2] H. C. Berg and D. A. Brown, Nature (London) **239**, 500 (1972).
[3] M. A. S. Vigeant, R. M. Ford, M. Wagner, and L. K. Tamm, Appl. Environ. Microbiol. **68**, 2794 (2002).
[4] E. Lauga, W. R. DiLuzio, G. M. Whitesides, and H. A. Stone, Biophys. J. **90**, 400 (2005).
[5] H. C. Berg and L. Turner, Biophys. J. **58**, 919 (1990).
[6] P. D. Frymier, R. M. Ford, H. C. Berg, and P. T. Cummings, Proc. Natl. Acad. Sci. U.S.A. **92**, 6195 (1995).
[7] M. Ramia, D. L. Tullock, and N. Phanthien, Biophys. J. **65**, 755 (1993).
[8] W. R. DiLuzio, L. Turner, M. Mayer, P. Garstecki, D. B. Weibel, H. C. Berg, and G. M. Whitesides, Nature (London) **435**, 1271 (2005).
[9] D. G. Jewett, T. A. Hilbert, B. E. Logan, R. G. Arnold, and R. C. Bales, Water Res. **29**, 1673 (1995).
[10] J. W. McClaine and R. M. Ford, Biotechnol. Bioeng. **78**, 179 (2002).
[11] J. R. Lawrence and D. E. Caldwell, Microb. Ecol. **14**, 15 (1987).
[12] Y. Xia and G. M. Whitesides, Angew. Chem., Int. Ed. Engl. **37**, 550 (1998).
[13] Here, the relative coordinate system for each surface is defined by a y axis pointing upstream of flow and a z axis pointing above the flow side of the surface, as depicted in Fig. 1. We adopt the convention that left denotes the $-x$ direction in the relative coordinate system for each surface.
[14] See EPAPS Document No. E-PRLTAO-98-004707 for supplementary movies. For more information on EPAPS, see http://www.aip.org/pubservs/epaps.html.
[15] This is mostly because the torque along the x direction on the cell body due to the shear flow will be larger than that due to flagellar propulsion at high shear flow rates.
[16] M. A. Mulvey, J. D. Schilling, J. J. Martinez, and S. J. Hultgren, Proc. Natl. Acad. Sci. U.S.A. **97**, 8829 (2000).
[17] L. E. Nicolle, Drugs & Aging **22**, 627 (2005).
[18] R. A. Garibaldi, J. P. Burke, M. R. Britt, W. A. Miller, and C. B. Smith, N. Engl. J. Med. **303**, 316 (1980).
[19] B. A. Macler and J. C. Merkle, Hydrogeol. J. **8**, 29 (2000).
[20] R. Taylor, A. Cronin, S. Pedley, J. Barker, and T. Atkinson, FEMS Microbiol. Ecol. **49**, 17 (2004).
[21] S. Park, P. M. Wolanin, E. A. Yuzbashyan, P. Silberzan, J. B. Stock, and R. H. Austin, Science **301**, 188 (2003).
[22] Y. H. An, J. B. McGlohorn, B. K. Bednarski, K. L. Martin, and R. J. Friedman, Methods Enzymol. **337**, 79 (2001).